Available online at www.sciencedirect.com
SCIENCE DIRECT
Journal of Molecular Catalysis A: Chemical 252 (2006) 17–22
JOURNAL OF MOLECULAR CATALYSIS A: CHEMICAL
www.elsevier.com/locate/molcata

A Fe-promoted Ni–P amorphous alloy catalyst (Ni–Fe–P) for liquid phase hydrogenation of *m*- and *p*-chloronitrobenzene

Xinhuan Yan [a,*], Junqing Sun [a], Youwen Wang [b], Jianfeng Yang [a]

[a] *State Key Laboratory Breeding Base of Green Chemistry-Synthesis Technology, Zhejiang University of Technology, Hangzhou 310014, PR China*
[b] *Center of Analysis & Measurement, Zhejiang University, Hangzhou 310027, PR China*

Received 22 August 2005; received in revised form 27 January 2006; accepted 30 January 2006
Available online 13 March 2006

Abstract

The Fe-doped Ni–P amorphous alloy catalyst was prepared by the chemical reduction of the aqueous solution containing $NiCl_2$ and $FeCl_3$ with NaH_2PO_2 at 343 K and characterized by EDS, XRD, SAED, TEM, XPS and DTA. It was used as a catalyst for the liquid phase hydrogenation of *m*-chloronitrobenzene (CNB) and *p*-chloronitrobenzene (CNB) to corresponding chloroaniline (CAN) in alcohol at 383 K under 1.0 MPa of hydrogen. At a suitable Fe content (X_{Fe}), the Ni–Fe–P amorphous alloy catalyst exhibited much higher activity and selectivity than the Ni–P, Fe–P, and Raney Ni catalysts in the hydrogenation reaction. With the increase of X_{Fe}, the activity first increased and then decreased. The optimum X_{Fe} was 0.25, at which the conversions of CNB could reach 99.9% and the yields of *m*- and *p*-CAN could reach 97.3% and 98.1%, respectively. The promoting effect of the Fe-dopant could be attributed to both a dispersing effect that resulted in the higher stability and the electron donation of the metallic Fe to the metallic Ni that was favorable for the hydrogenation. The structure of amorphous alloy and the alloying P were also favorable for the hydrogenation. Very high contents of the Fe-dopant ($X_{Fe} > 0.25$) resulted in the decrease of the hydrogenation activity because Ni active sites were mostly covered by the inactive Fe.

Keywords: Ni–Fe–P; Amorphous alloy; Chloronitrobenzene; Chloroaniline; Liquid phase hydrogenation

1. Introduction

Halogenated anilines are important intermediates for synthesis of organic fine chemicals, such as dyes, drugs, herbicides, and pesticides. The main routes to their production involve the Bechamp reaction in a metal acid system, or selective hydrogenation over heterogeneous catalysts. The hydrogenation is now preferred, owing to its lower impact on the environment since no acid effluents are produced. The catalysts for the hydrogenation have been well-studied, such as platinum [1,2], palladium [3], rhodium [4], nickel [5], and copper chromite [6] catalysts. Among these, platinum shows better selectivity of halogenated aniline and a fast rate of reduction of the nitro-group. But it is always accompanied by some hydrogenolysis of the carbon–halogen bond. Depending on the halogen and its position relative to the nitro group in the halogenated nitrobenzene, dehalogenation can vary from negligible to near 100%. To improve the hydrogenation selectivity, the catalyst preparations are modified (alloying [7] and metal/support interaction [8–10], etc.) or specific additives (promoters or inhibitors) [11,12] are used in the reaction system. But none of the catalysts previously proposed are satisfactory, each having its own particular limitations.

During the past decades, amorphous alloy catalysts have been widely used in the hydrogenation owing to their higher activity, better selectivity, and stronger poisoning resistance [13,14]. Up to now, a great number of systematic studies have been made on metal-B amorphous alloy catalysts [15–19], but quite limited work has been done on the metal-P amorphous alloy catalysts [20]. In this paper, we report novel Fe-doped Ni–P amorphous alloy catalysts (Ni–Fe–P) which exhibited both excellent activity and selectivity in liquid phase hydrogenation of *m*-chloronitrobenzene (CNB) and *p*-chloronitrobenzene (CNB) to corresponding chloroaniline (CAN). The effect of the Fe content on the catalytic activity was investigated; results demonstrated that the optimum Fe/(Ni + Fe) molar ratio was

* Corresponding author. Tel.: +86 571 8832 0791; fax: +86 571 8832 0791.
E-mail address: whh97@sina.com (X. Yan).

1381-1169/$ – see front matter © 2006 Elsevier B.V. All rights reserved.
doi:10.1016/j.molcata.2006.01.060

0.25. Based on various characterizations, the promoting effect of the Fe dopant on both the catalytic activity and selectivity was discussed briefly.

2. Experimental

2.1. Catalyst preparation

The Ni–Fe–P amorphous alloy catalysts were prepared by the chemical reduction of the aqueous solution that consisted of $NiCl_2{\cdot}6H_2O$, $FeCl_3$, $NaH_2PO_2{\cdot}H_2O$ and CH_3COONa. The initial molar ratio of NaH_2PO_2 to metallic salts was 3:1. The pH value of solution was adjusted to 11 using 30 wt.% NaOH aqueous solution. The solution was kept at 343 K with vigorous stirring until the evolution of a gas ceased. The resulting black solid was washed thoroughly with 8 M aqueous ammonia and distilled H_2O until it was free from Cl^- ion. Then, it was further washed with absolute alcohol (EtOH) and finally stored in EtOH until the time of use. The content of the Fe-dopant in the Ni–Fe–P sample, expressed as X_{Fe} (%), the molar ratio of Fe/(Ni + Fe), was adjusted by changing the initial molar ratio of Ni/Fe in the solution. For comparison, the Ni–P ($X_{Fe} = 0$) and the Fe–P ($X_{Fe} = 1$) samples were also prepared in a similar way but using single $NiCl_2{\cdot}6H_2O$ or $FeCl_3$ as the catalyst precursor. Raney Ni catalyst was also prepared by alkali leaching of the commercially available Ni–Al alloy (50 wt.% Ni, 200 meshes), as described elsewhere [21].

2.2. Catalyst characterization

The composition of the as-prepared Ni–Fe–P catalyst was analyzed by X-ray energy dispersive spectroscopy (EDS, Thermo Noran Vantage ESI X). Its amorphous structure was confirmed by both the X-ray diffraction (XRD, Thermol ARL X'Tra with Cu Kα radiation) and selected area electron diffraction (SAED, JEOL JEM-200C). Transmission electron micrograph (TEM, JEOL JEM-200C) was used to determine the surface morphology and the particle size. The thermal stability of amorphous alloy was also studied by differential thermal analysis (DTA, Pyris Diamond, heating rate = 10 K/min). The surface electronic states were determined with a X-ray photoelectron spectroscope (XPS, Perkin-Elmer PH I 5000C). Slight Ar^+ sputtering was employed to remove surface impurities. All binding energy (BE) values were calibrated by using the value of contaminant carbon (C 1s = 284.6 eV) as a reference.

2.3. Activity test

Liquid phase hydrogenation of *m*-CNB or *p*-CNB was conducted as follows: 100 ml EtOH, 5.0 g *m*-CNB or *p*-CNB, 0.5 g catalyst were mixed in a 500 ml steel autoclave equipped with a mechanical stirrer and an electric heating system. The reactor was filled with H_2 eight times in succession to exclude the inside air. Then it was filled with H_2 up to 1.0 MPa, followed by heating slowly (110 K/h) until 383 K. When the hydrogen pressure reached a steady state, the hydrogenation was started immediately by stirring the reaction mixture vigorously. The stirring rate was kept at 1000 rpm to eliminate the diffusion effects. According to the drop of H_2 pressure with the time, the hydrogen uptake rates, i.e. the hydrogen consumption per hour and per gram Ni (R_{H_2}, mmol H_2/h g Ni) were calculated according to the ideal gas equation. The reaction products were analyzed by gas chromatography (Fuli 9790) from which the CNB conversion and the yield of CAN were obtained. The capillary column SE-54 with an i.d. of 0.32 mm and a length of 30 m equipped with an FID detector was used. Reactants and products were identified by comparison with authentic samples. Biphenyl was used as an internal standard.

3. Results and discussion

3.1. Catalysts characterization

The bulk compositions of the as-prepared Ni–P, Ni–Fe–P, and Fe–P amorphous alloy samples determined by EDS analysis are given in Table 1.

The XRD pattern of the fresh Ni–Fe–P-3 sample with $X_{Fe} = 0.25$, as shown in Fig. 1a, revealed that the sample was present in the amorphous structure, since only one broad peak around $2\theta = 45^\circ$ appeared [22]. Similar XRD patterns were also obtained for other Ni–Fe–P samples with X_{Fe} from 0% to 100%, indicating that the addition of the Fe-dopant did not change the amorphous structure. No appreciable change in the XRD pattern was observed when the Ni–Fe–P-3 was treated at a temperature below 473 K. However, a sharp diffractional peak appeared

Table 1
The compositions of the as-prepared Ni–Fe–P catalysts

Catalyst	X_{Fe} (molar ratio)	Composition (at.%)
Ni–P	0	$Ni_{78.2}P_{21.8}$
Ni–Fe–P-1	0.16	$Ni_{65.9}Fe_{12.9}P_{21.2}$
Ni–Fe–P-2	0.20	$Ni_{62.6}Fe_{15.8}P_{21.6}$
Ni–Fe–P-3	0.25	$Ni_{58.7}Fe_{19.6}P_{21.7}$
Ni–Fe–P-4	0.49	$Ni_{40.0}Fe_{39.0}P_{21.0}$
Ni–Fe–P-5	0.68	$Ni_{25.0}Fe_{53.0}P_{22.0}$
Ni–Fe–P-6	0.77	$Ni_{18.0}Fe_{59.8}P_{22.2}$
Fe–P	1.0	$Fe_{78.3}P_{21.7}$

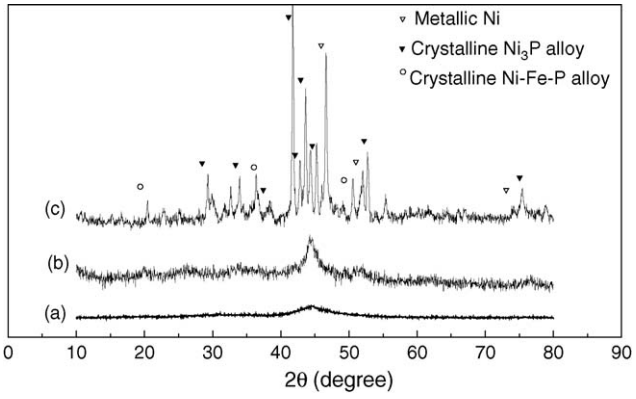

Fig. 1. XRD patterns of the Ni–Fe–P-3 sample treated at different temperatures: (a) fresh sample; (b) after treated at 473 K for 2 h in N_2 flow; (c) after treated at 873 K for 2 h in N_2 flow.

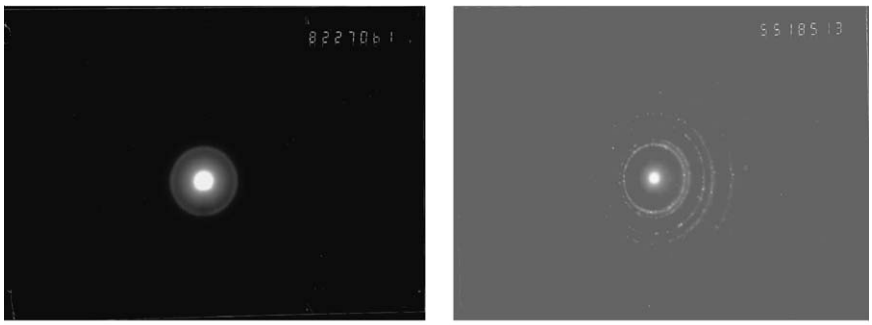

(a) (b)

Fig. 2. SAED patterns of the Ni–Fe–P-3 sample treated at different temperatures: (a) fresh sample; (b) after treated at 873 K for 2 h in N_2 flow.

when it was treated at 473 K in N_2 for 2 h, as shown in Fig. 1b, indicating the beginning of the crystallization. Both the intensity and the number of the diffractional peaks increased with the increase of the treating temperature, showing the increase in the crystallinity. By the treatment at 873 K in N_2 for 2 h, the crystallization reached completion since no more changes in the XRD patterns were observed when the treating temperature further increased. As shown in Fig. 1c, various diffractional peaks indicative of crystalline Ni_3P alloy, Ni–Fe–P alloy, and metallic Ni phases appeared in the XRD pattern when the Ni–Fe–P-3 sample was treated at 873 K in N_2 for 2 h, showing that the amorphous structure was thermodynamically metastable and that the as-prepared Ni–Fe–P-3 underwent a crystallization together with a decomposition at high temperature.

The amorphous structure of the fresh Ni–Fe–P-3 sample was further confirmed by the SAED pattern. As shown in Fig. 2a, the fresh sample displayed a series of diffractional circles indicative of typical amorphous structure [23]. After the sample was treated at 873 K in N_2 for 2 h, these diffractional circles disappeared and only separated bright dots were observed, as shown in Fig. 2b, which demonstrated the crystallization of the Ni–Fe–P-3 sample.

In order to evaluate the electronic state of the as-prepared Ni–Fe–P amorphous alloy, the BE of the substance was determined by XPS. Fig. 3 shows the XPS spectra of the fresh Ni–Fe–P-3 sample. From the Ni $2p_{3/2}$ energy level, one could see that almost all the Ni species were present in the metallic state with the BE around 853.1 eV, the same as that of the pure metal Ni [24]. However, the Fe species were present in both the metallic state and the oxidized state (Fe_2O_3) corresponding to BE of 707.6 and 711.6 eV, respectively. In comparison with the standard BE of pure Fe metal (707.0 eV), the BE of the metallic Fe in the Ni–Fe–P-3 positively shifted about 0.6 eV, indicating that the metallic Fe donated partial electron to the metallic Ni, i.e. the metallic Fe was electron-deficient while the metallic Ni was electron-enriched. From the P 2p level, the P species in the Ni–Fe–P-3 sample were present in the alloying state with the BE around 130.1 eV. By comparing with the standard BE of the pure red phosphorus (130.1 eV) [24], it was found that no electron transfer took place between Ni and P, which was in agreement with Deng et al. [25]. This indicates that electronic interaction between Ni and P in the Ni–Fe–P-3 was not important.

According to DTA analysis, as shown in Fig. 4, the crystallization temperature of the samples strongly depended on X_{Fe}. The crystallization temperature of the Ni–Fe–P-1 sample at $X_{Fe} = 0.16$ was nearly 46 K higher than that of the Ni–P sample. With the increase of X_{Fe}, the crystallization temperature increased rapidly mainly owing to the presence of Fe_2O_3 support, which effectively inhibited the aggregation of particles during the heating treatment. It clearly demonstrated the stabilizing effect of the Fe-dopant on the amorphous alloy structure.

The TEM was employed to show the shape and the size of the fresh Ni–Fe–P-3 sample and the fresh Ni–P sample, as shown in Fig. 5. It confirmed that the fresh Ni–Fe–P-3 sample was present in the form of spherical particles with the size ranging from 30 to 120 nm and the fresh Ni–P sample was also in the form of spherical particles with the size ranging from 60 to 180 nm. The particles in the fresh Ni–Fe–P-3 sample were smaller and distributed more homogeneously than the fresh Ni–P sample mainly owing to the dispersing effect of the Fe_2O_3 and the strong interaction between the Ni–P amorphous alloy particles and the Fe-dopant.

3.2. Catalytic properties for the selective hydrogenation of m- and p-CNB

The liquid phase hydrogenation of CNB was a complicated process, and many by-products were involved. It followed the reaction pathways described in the literature [26]. Our purpose was to achieve high selectivity to CAN without the hydrogenolysis of the C–Cl bond. We investigated the effect of different Fe amounts on the hydrogenation of *m*- and *p*-CNB over Ni–Fe–P amorphous alloy catalyst. The results were listed in Tables 2 and 3.

From Tables 2 and 3, it could be seen clearly that Ni–Fe–P amorphous catalyst exhibited higher activity and selectivity in the hydrogenation of CNB than Ni–P, Fe–P, and Raney Ni catalysts. As shown in Fig. 6, the initial catalytic activity (R_{H_2}) increased remarkably when a small amount of Fe was added to the Ni–P catalyst. With the increase of X_{Fe}, R_{H_2} first increased and then decreased. The maximum activity was obtained at $X_{Fe} = 0.25$.

Addition of Fe in Ni–P catalyst also had significant influence on the conversions of *m*- and *p*-CNB and the yields of *m*- and *p*-CAN. When $X_{Fe} = 0.25$, the conversions of *m*- and *p*-CNB could

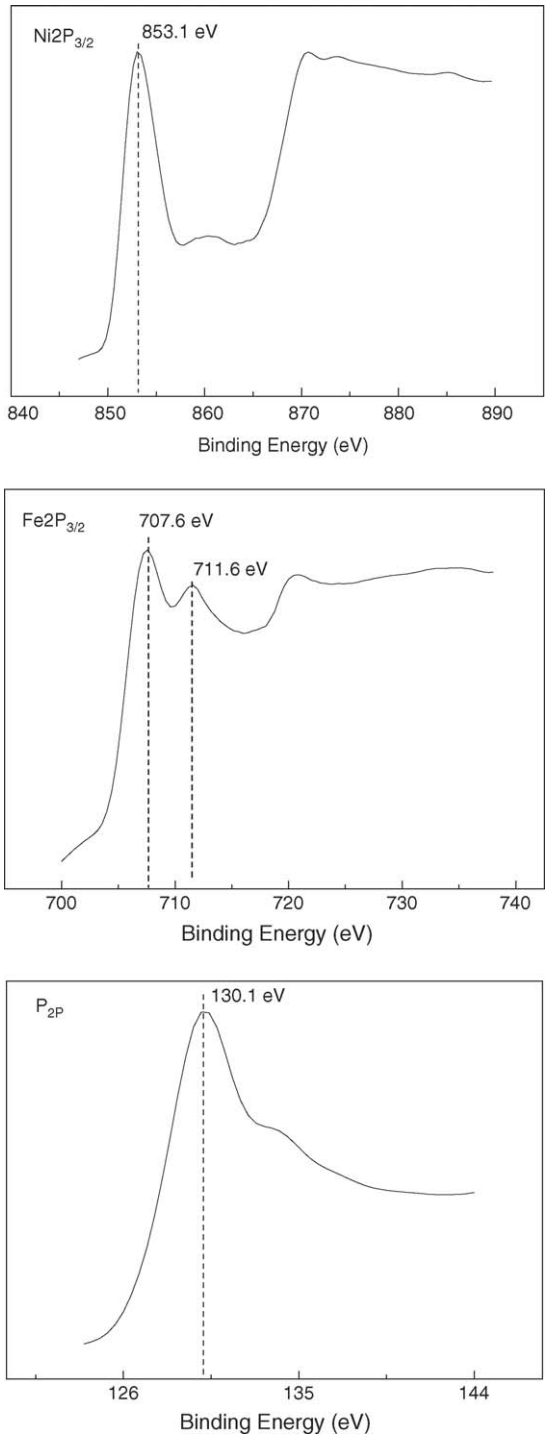

Fig. 3. XPS spectra of the Ni–Fe–P-3 amorphous alloy catalyst.

all reach 99.9% while the yield of *m*-CAN could reach 97.3% and the yield of *p*-CAN could reach 98.1%.

It was known [27] that the rate determining step of this type of heterogeneously catalysed reaction was a nucleophilic attack of hydride ion, produced by dissociative adsorption of H_2 molecule on the metal surface, on the nitrogen atom of the nitro group. Therefore, electron withdrawing and electron donating effects of the substituents might have a strong influence on the reactivity of CNB.

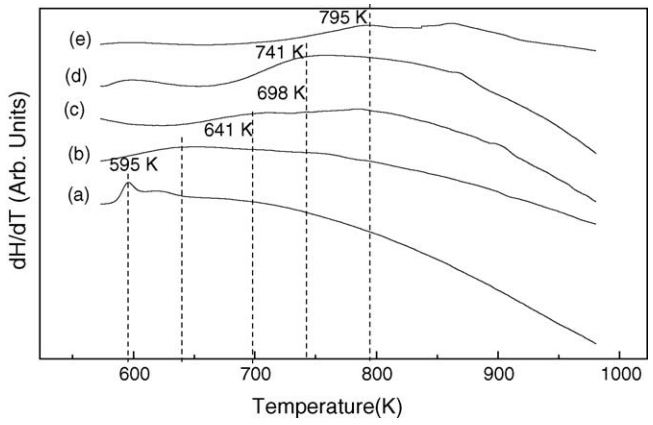

Fig. 4. DTA curves of: (a) Ni–P; (b) Ni–Fe–P-1; (c) Ni–Fe–P-3; (d) Ni–Fe–P-5; (e) Fe–P samples obtained under the same preparation conditions.

Table 2
Catalytic properties for the liquid phase hydrogenation of *m*-CNB over the as-prepared Ni–Fe–P catalyst and Raney Ni catalysts[a]

Catalyst	R_{H_2} (mmol/h g Ni)	Conversion (%)	Yield of productions (mol.%)[b]		
			AN	NB	*m*-CAN
Ni–P	51.4	99.4	2.6	0.2	92.6
Ni–Fe–P-1	56.7	94.3	1.8	0.9	90.9
Ni–Fe–P-2	68.9	96.5	1.7	0.3	93.5
Ni–Fe–P-3	95.1	99.9	1.5	–	97.3
Ni–Fe–P-4	41.0	75.3	0.3	0.2	72.7
Ni–Fe–P-5	29.9	60.1	–	–	58.6
Ni–Fe–P-6	22.8	49.9	–	–	49.7
Fe–P	10.2	20.8	–	–	19.3
Raney Ni	89.1	95.2	16.3	2.0	81.4

[a] Reaction conditions: 0.5 g catalyst; 5.0 g *m*-CNB; 100 ml EtOH; P_{H_2} = 1.0 MPa; T = 383 K; stirring rate = 1000 rpm.
[b] Some products with high boiling point could not be determined by GC analysis. AN: aniline; NB: nitrobenzene.

As the Fe–P amorphous alloy itself was inactive for the liquid phase hydrogenation of CNB, according to Tables 2 and 3, one could conclude that, at a suitable amount of the Fe-dopant, Fe served as a promoter in the Ni–Fe–P amorphous alloy and the active site was the metallic Ni. The promoting effect of the

Table 3
Catalytic properties for the liquid phase hydrogenation of *p*-CNB over the as-prepared Ni–Fe–P catalyst and Raney Ni catalysts[a]

Catalyst	R_{H_2} (mmol/h g Ni)	Conversion (%)	Yield of productions (mol.%)		
			AN	NB	*p*-CAN
Ni–P	47.6	99.2	2.3	–	93.6
Ni–Fe–P-1	61.5	99.5	4.3	0.2	91.5
Ni–Fe–P-2	72.2	99.6	3.7	0.9	93.8
Ni–Fe–P-3	93.3	99.9	1.2	–	98.1
Ni–Fe–P-4	57.9	83.6	0.9	0.3	80.9
Ni–Fe–P-5	40.3	70.5	1.0	0.8	63.7
Ni–Fe–P-6	33.6	63.2	–	–	62.5
Fe–P	11.7	25.7	–	–	24.7
Raney Ni	85.0	96.0	11.7	1.6	84.2

[a] Reaction conditions are similar to Table 2.

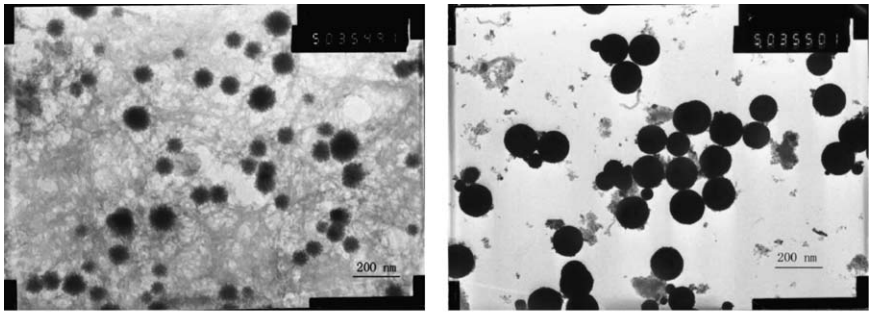

Fig. 5. TEM images of: (a) fresh Ni–Fe–P-3; (b) fresh Ni–P.

Fe-dopant may be accounted for by considering the presence of both the metallic Fe and the Fe_2O_3. As the aforementioned XPS spectra revealed that the metallic Fe donated partial electrons to Ni, the Fe atoms were electron-deficient and Ni atoms were electron-enriched in the Ni–Fe–P amorphous alloy catalyst. The electron-deficient Fe could attract the oxygen in the nitrogen–oxygen bond, which might activate the polar NO_2 groups of CNB and coordinate with the NH_2 groups of produced CAN molecules, thereby promoting the hydrogenation of CNB and depressing the dehalogenation of CAN. For the mechanism in the hydrodehalogenation reaction of aromatic halides, most researchers agreed that there was an electrophilic attack of cleaved hydrogen on the adsorbed aromatic halides [28,29]. The electron-deficient Fe atoms could weaken the extent of electron feedback from the Ni atoms to the aromatic ring in CAN, which would further suppress the hydrodechlorination of CAN. But a large concentration of the Fe-dopant was harmful to the activity, because surface Ni active sites would be mostly covered by the inactive Fe-dopant.

The excellent activity and selectivity of the Ni–Fe–P catalyst could also be attributed to the structural effect and the alloying P. For the structural effect, it had been claimed that the amorphous alloy had unique long-distance disordering but only short-distance ordering structure, and had unique isotropic structure and high concentration of coordinatively unsaturated sites [30,31], which were favorable for most hydrogenation reactions [14,32]. Other structural parameters, such as the highly unsaturated property of the Ni active sites, the strong synergistic effect between the different Ni active sites, and the uniform distribution of the Ni active sites, also promoted the hydrogenation activity [33]. From Tables 2 and 3, one could conclude that the Ni–P amorphous alloy catalyst exhibited much better selectivity to CAN than the Raney Ni catalyst, showing the promoting effect of the alloying P on the catalytic behaviors. But the mechanism is still not clear now. Studies on the details of the catalytic mechanism of the promising Ni–Fe–P amorphous alloy catalyst in this work are being continued.

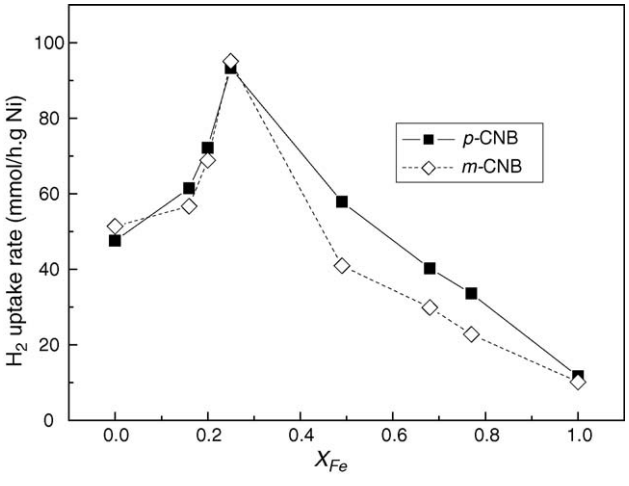

Fig. 6. Dependence of the hydrogenation activity of the Ni–Fe–P amorphous catalyst on the Fe/(Ni + Fe) molar ratio (X_{Fe}). Reaction conditions are given in Table 2.

4. Conclusion

Based on the above results, it was clarified that at a suitable content of the Fe-dopant (X_{Fe}), the Ni–Fe–P amorphous alloy catalyst displayed excellent catalytic properties for the liquid phase hydrogenation of CNB to corresponding CAN. The optimum X_{Fe} was 0.25. The conversions of *m*- and *p*-CNB were all over 99.9% while the yields of *m*- and *p*-CAN were 97.3% and 98.1% respectively over the Ni–Fe–P amorphous catalyst with $X_{Fe} = 0.25$. On one hand, the promoting effect of the Fe-dopant could be attributed to a dispersing effect that could inhibit the aggregation of Ni–Fe–P alloy particles and, in turn, could increase the stability of the Ni–Fe–P amorphous alloy. On the other hand, the promoting effect of the Fe-dopant was also attributed to the electron interactions between Fe and Ni. Electron-deficient Fe promoted the activity of the Ni atoms by activating the polar NO_2 groups of CNB and coordinating with the NH_2 groups of produced of CAN molecules, thereby promoting the hydrogenation of CNB and depressing the dehalogenation of CAN. The Fe-dopant could weaken the extent of electron feedback from the Ni atoms to the aromatic ring in CAN, which would further suppress the hydrodechlorination of CAN. Meanwhile, the structure of amorphous alloy and the alloying P were favorable for the liquid phase hydrogenation of CNB. The results described here showed that the Ni–Fe–P amorphous alloy catalyst was a promising catalyst for industrial application.

Acknowledgements

This work was supported by the National Natural Science Foundation of China (20276071) and the Special Natural Science Foundation of Zhejiang (ZE0102).

References

[1] J.R. Kosak, US Patent 4,020,107 (1977) to E.I. du Pont de Nemours and Co.
[2] L. Cerveny, I. Paseka, V. Struckly, V. Ruzicka, Collect. Czech. Chem. Commun. 47 (1982) 853.
[3] R. Baltzly, A.P. Phillips, J. Am. Chem. Soc. 68 (1946) 261.
[4] W.P. Dunworth, F.F. Nord, J. Am. Chem. Soc. 74 (1952) 1459.
[5] C.F. Winans, J. Am. Chem. Soc. 61 (1939) 3564.
[6] B.O. Pray, F.C. Trager, US Patent 2,791,613 (1957) to Columbia-Southern Chemical.
[7] B. Coq, A. Tijani, F. Figueras, J. Mol. Catal. 71 (1992) 317.
[8] M.H. Liu, W.Y. Yu, H.F. Liu, J. Mol. Catal. A 138 (1999) 295.
[9] W.X. Tu, H.F. Liu, Y. Tao, J. Mol. Catal. A 159 (2000) 115.
[10] J.L. Zhang, Y. Wang, H. Ji, Y.G. Wei, N.Z. Wu, B.J. Zuo, Q.L. Wang, J. Catal. 229 (2005) 114.
[11] X.X. Han, R.X. Zhou, X.M. Zheng, H. Jiang, J. Mol. Catal. A 193 (2003) 103.
[12] X.X. Han, R.X. Zhou, G.H. Lai, B.H. Yue, X.M. Zheng, J. Mol. Catal. A 209 (2004) 83.
[13] A. Molnar, G.V. Smith, M. Bartok, Adv. Catal. 36 (1989) 329.
[14] A. Baiker, Faraday Discuss. Chem. Soc. 87 (1989) 239.
[15] Z. Jiang, H.W. Yang, Z. Wei, Z. Xie, W.J. Zhong, S.Q. Wei, Appl. Catal. A 279 (2005) 165.
[16] B.J. Liaw, S.J. Chiang, C.H. Tsai, Y.Z. Chen, Appl. Catal. A 284 (2005) 239.
[17] H.X. Li, Y.D. Wu, J. Zhang, W.L. Dai, M.H. Qiao, Appl. Catal. A 275 (2004) 199.
[18] L.J. Wang, W. Li, M.H. Zhang, K.Y. Tao, Appl. Catal. A 259 (2004) 185.
[19] J. Fang, X.Y. Chen, B. Liu, S.R. Yan, M.H. Qiao, H.X. Li, H.Y. He, K.N. Fan, J. Catal. 229 (2005) 97.
[20] H.X. Li, Y.P. Xu, Mater. Lett. 51 (2001) 101.
[21] H.X. Li, W.J. Wang, H. Li, J.F. Deng, J. Catal. 191 (2000) 257.
[22] H. Yamashita, M. Yoshikawa, T. Funabiki, S. Yoshida, J. Chem. Soc., Faraday Trans. I 82 (1986) 1771.
[23] S. Klein, J.A. Martens, R. Parton, K. Vercruysse, P.A. Jacobs, W.F. Maier, Catal. Lett. 38 (1996) 209.
[24] H. Li, H.X. Li, W.L. Dai, W.J. Wang, Z.J. Fang, J.F. Deng, Appl. Surf. Sci. 152 (1999) 25.
[25] J.F. Deng, H. Chen, X. Bao, M. Muhler, Appl. Surf. Sci. 81 (1994) 341.
[26] W. Pascoe, in: P.N. Rylander, H. Greenfield, R.L. Augustine (Eds.), Catalysis of Organic Reactions, Marcel Dekker, New York, 1988, p. 121.
[27] P. Lu, N. Toshima, Bull. Soc. Jpn. 73 (2000) 751.
[28] B. Coq, A. Tijani, R. Dutartre, F. Figueras, J. Mol. Catal. 79 (1993) 253.
[29] C. Menini, C. Park, E.J. Shin, G. Tavoularis, M.A. Keane, Catal. Today 62 (2000) 355.
[30] Y. Chen, Catal. Today 44 (1998) 3.
[31] X.Y. Chen, S. Wang, J.H. Zhuang, M.H. Qiao, K.N. Fang, H.Y. He, J. Catal. 227 (2004) 419.
[32] J.F. Deng, H.X. Li, W.J. Wang, Catal. Today 51 (1999) 113.
[33] B. Shen, S. Wei, K. Fan, J.F. Deng, Appl. Phys. A 65 (1997) 295.